北海道大学工学部研究報告
第 128 号 (昭和 60 年)

Bulletin of the Faculty of Engineering,
Hokkaido University. No.128 (1985)

On the Triaxial Compression Test of Coal and Other Specimens in Which high Pressure Gas is Involved

Masuyuki UJIHIRA*, Kiyoshi HIGUCHI* and Hideki MIZUMA**

(Received June 30, 1985)

Abstract

In general, where the differential stress $\sigma_1-\sigma_2$ has a large value in a coal seam at the back of an underground working face, such a portion may readily be susceptible to failure by rock pressure.

When such a part of the coal seam contains high pressure gas in its pores and fissures, the coal seam fracturing may be affected not only by rock pressure but also by gas pressure. To examine the gas pressure influence to the failure stress of coals or mortar, triaxial compression tests of them to which gas pressure was applied to pores and fissures were conducted.

It was found experimentally that when the pore gas pressure was raised under constant confining pressure, the strength (failure stress) decreased reversely as well as in the case when pore pressure was applied by water. These results mean that, in underground drift driving, the higher the coal seam gas pressure becomes the more the coal seam or rock becomes susceptible to failure under the same rock pressure condition.

1. Introduction

The objective of the experimental study described in this paper was to determine whether the coals or other mortar materials retaining high pressure gas in their pores and fissures might have a lower strength than those having no pore pressure in the triaxial compression test. As shown in Figure 1, if the pore gas pressure of the material P_p is raised in the triaxial stress state, Mohr's circle III might move to the position of Mohr's circle II following to the Law of Effective Stress as recognized in soil mechanics, the latter circle might touch or cross the envelope and the material might rupture[1]. Here,

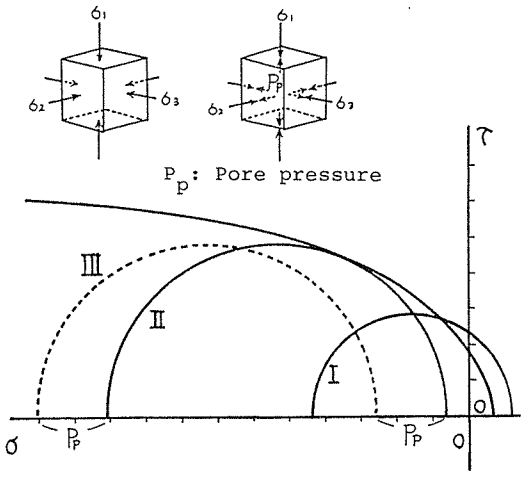

Figure 1 Schema for explaining the Law of Effective Stress

* Dep. of Mineral Resources Development Eng., Sapety Eng..
** The Science and Technology Agency.

Mohr's parabolic envelope is assumed as a failure criterion.

Conventionally, triaxial compression tests to which pore water pressure was applied has been conducted[2)3)4)]. Because, when the problems of coal and gas outbursts etc are studied, pore fluid pressure should be given by gas, thus the authors carried out triaxial compression test applying pore pressure by gas and attempted to confirm the aforesaid effect of pore gas pressure against compressive strength of coals.

2. Material studied

Size and mechanical characteristics of three dissimilar coals and one kind of mortar are given in Table 1. The average length of coal test pieces was 50 mm and the average diameter of those was 30 mmϕ. Average size of mortar test pieces was 96.3×50.0 mm ϕ. Each test piece was previously dried for at least one month under natural room humidity and temperature conditions.

Table 1. Mechanical properties of employed materials

	COAL-POWDER MORTAR	COAL (TAIHEIYO)	COAL (HORONAI)	COAL (SORACHI)
size (mm)	96.3×50.0ϕ	48.4×30.0ϕ	50.6×30.0ϕ	50.2×30.0ϕ
compressive strength (kg/cm^2)	120.4	290.9	140.3	139.5
tensile strength (kg/cm^2)	5.20	9.37	13.5	5.42
porosity (%)	22.4	11.1	12.4	9.7
specific weight	1.46	1.20	1.22	1.21
p.w. velocity (m/sec.)	2.02×10^3	1.92×10^3	1.90×10^3	1.39×10^3
s.w. velocity (m/sec.)	9.58×10^2	7.16×10^2	9.61×10^2	8.39×10^2

3. Experimental procedure

For the triaxial compression tests, the apparatus shown in Figure 2 was used. Instead of oil, the confining pressure was applied by nitrogen gas. Pore gas pressure was applied from another N_2 gas bomb through a copper tube and steel made bottom end-piece. Both the load and axial displacement were detected by loadcell and dialgauge respectively and they were recorded by a X-Y recorder, then a stress-strain curve was drawn.

Correctly shaped test piece was slightly coated by an adhesive agent to its surface, rolled fast by a vinyl tape and sandwiched between the upper and bottom end-pieces. Then the test piece and two end-pieces were rolled together on their surface again by vinyl tape and pasted by silicon grease heavily. The end-pieces had ten grooves of which depth and pitch were 1 mm respectively. These treatments prevented gas leakage from the vessel to the inner part of the test piece. After a test piece was set in the vessel, platen of compression testing machine was contacted softly on the piston for loading, then the confining pressure P_c was given. Gas leakage from the vessel to the inner part of the test piece through coating was

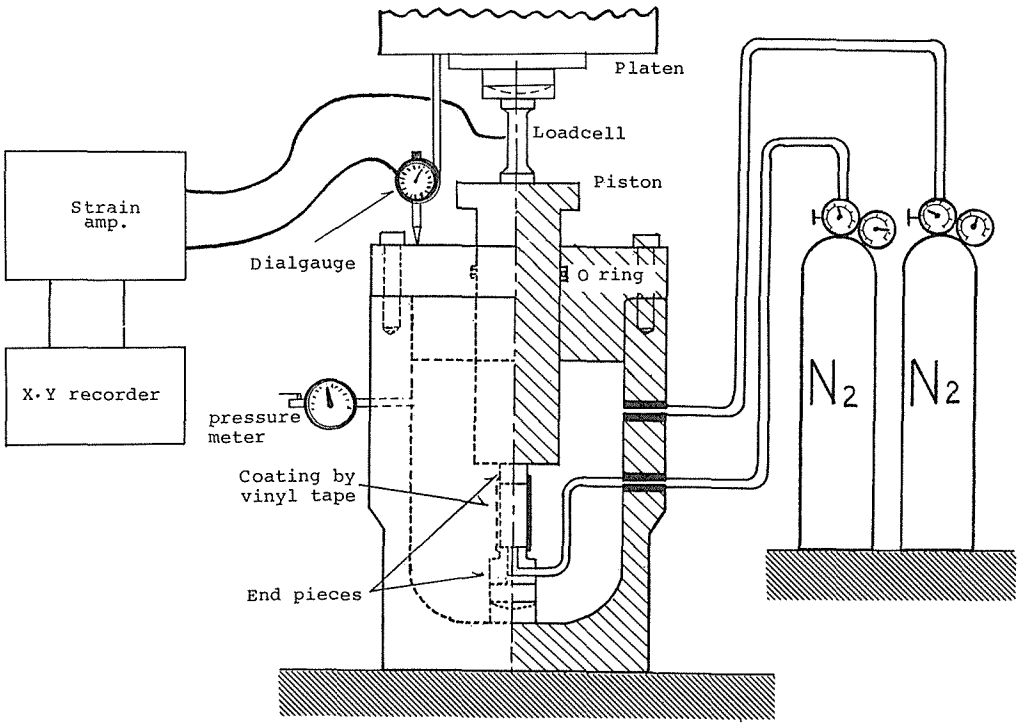

Figure 2 Experimental apparatus for triaxial compression test

examined by a gas pressure meter attached to the pore gas flow circuit. Finally, the pore gas pressure P_p was applied and the compression test was carried out.

Here, a numerical calculation was conducted to evaluate the amount of time required for attaining gas pressure equilibrium in the entire interior parts of the test piece. For calculation, measured gas permeability of Taiheiyo coal $K=5\times10^{-3}$ darcy was used. The result of the calculation shows that, at all gas pressure levels, the gas pressure equilibrium could be attained only within 10 seconds (Figure 3). For practical purposes the triaxial compression test was conducted after one hour pore gas pressurization. The rate of strain $\dot{\varepsilon}$ was controlled to 590×10^{-6}/sec.

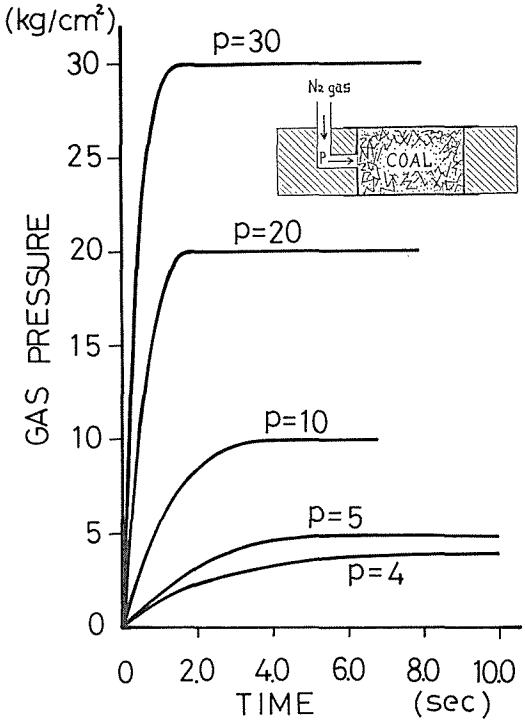

Figure 3 Time required for getting gas pressure equilibrium in the entire interior parts of test piece

4. Experimental results

4-1 Natures of fracture

Figure 4, 5, 6 and 7 show the stress-strain curves of Taiheiyo coal, Sorachi coal, Horonai coal and mortar respectively.

These figures show when the types of material were dissimilar, and the nature of fracture was also different among them as follows.

(1) Taiheiyo coal which has no danger for coal and gas outbursts showed a typical brittle fracture from (Figure 4). In every pressure range (P_c=40 K Pc=40 Kg/cm², Pp=0−40 Kg/cm²), this coal showed only brittle type fracture.

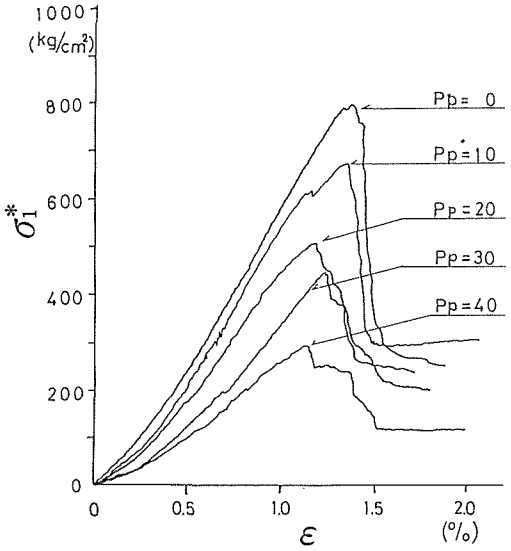

Figure 4 Stress-Strain curve of Taiheiyo coal

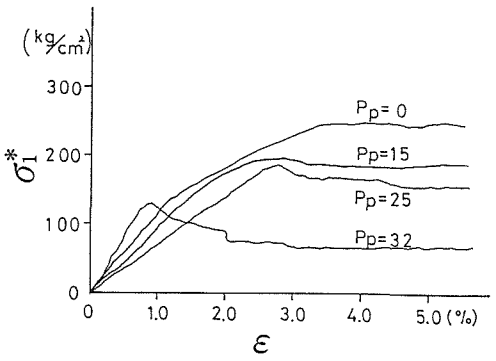

Figure 5 Stress-Strain curve of Sorachi coal

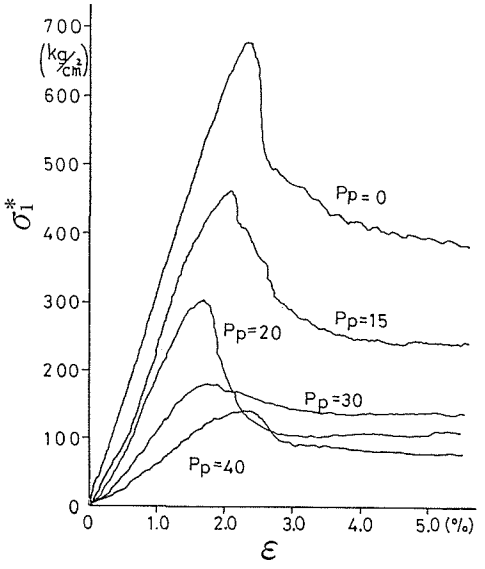

Figure 6 Stress-Strain curve of Horonai coal

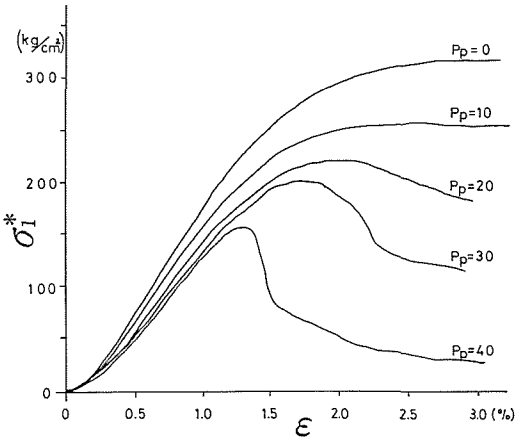

Figure 7 Stress-Strain curve of mortar

(2) Sorachi coal which was sampled from an outburst prone seam has stress-strain curves for ductile or transitional fracture (Figure 5). In this case, when the pore gas pressure P_p was 0, it appeared ductile fracturing behavior.

When the pore pressure was set in the range of more than 25 Kg/cm^2, the fracturing behavior changed from ductile to transitional fracture form.

(3) Horonai coal which is not an outburst prone coal has stress-strain curves for transitional type fracture. Regardless of the pressure level of pore gas, only transitional type fractures occurred (Figure 6).

(4) Soft mortar has stress-strain curves for ductile or transitional fracture (Figure 7).

Until the pore gas pressure P_p was lower than 10 Kg/cm^2, fracturing behavior was ductile. When the pressure P_p was increased to more than 10 Kg/cm^2 stepwise, the fracturing behavior changed gradually to transitional fracture.

As mentioned above, it can be said that when the pore gas pressure is applied to weak materials, the fracturing behavior is tends to change from ductile to brittle type fractures.

4-2 Relation between pore gas pressure and compressive strength

In every test, confining pressure was set as constant (P_c=40 Kg/cm^2) and only pore gas pressure was changed.

Table 2 shows the results of triaxial test of Taiheiyo coal. Taiheiyo coal was hard ; average uniaxial strength was 290.8 Kg/cm^2, average tensile strength was 9.4 Kg/cm^2 and porosity was 11.1 %. The relation between $\sigma_3^*(=P_c-P_p)$ and failure stress $\sigma_1^*(=\sigma_1-P_p)$ is shown in Figure 8. The strength when $\sigma_3^*=0$ was about 1/3 of the strength at $\sigma_3^*=40$ Kg/cm^2 as compared with the most far apart values in Table 2. The triaxial strength when $\sigma_3^*=0$ was almost equal to the uniaxial compressive strength that was marked with white circles in Figure 8.

Table 3 shows the triaxial compressive strength of Sorachi coal. The average uniaxial strength of the coal was 139.5 Kg/cm^2, the average tensile strength was 5.4 Kg/cm^2 and porosity was 9.7 %. Figure 9 shows the relation between σ_3^* and σ_1^*. The same as in the case of Taiheiyo coal, when the pore gas pressure was increased under the constant confining condition P_c=40 Kg/cm^2, triaxial compressive strength clearly decreased.

Table 4 shows the results of triaxial compression test of Horonai coal. Uniaxial compressive strength of Horonai coal was lower than that of Taiheiyo coal and higher than that of Sorachi coal.

The average uniaxial compressive strength was 140.3 Kg/cm^2, the average tensile strength was 13.5 Kg/cm^2 and the porosity was 12.4 %. Figure 10 shows the relation between σ_3^* and σ_1^*. The same as in the case of Taiheiyo and Sorachi coals, when the pore gas pressure was increased stepwise, the triaxial compressive strength decreased conversely.

The triaxial compressive strength when $\sigma_3^*=0$ was about 10/97 of the strength at $\sigma_3^*=40$ Kg/cm^2 as compared to the most far apart values in Table 4. The influence of the pore gas pressure was clearly confirmed. As mentioned in the above 2 examples, the triaxial strength at $\sigma_3^*=0$ was similar to the uniaxial strength as plotted by white circles in Figure 10.

Table 2. Results of triaxial compresion test of Taiheiyo coal

No.	P_c	P_p	$\sigma_3^*(P_c-P_p)$	σ_1^*	Young's modulus ($\times 10^4$)	comment
1	40	40	0	287	1.69	Sc=290.8
2	40	40	0	291	1.78	
3	40	40	0	389	1.69	St= 9.37
4	40	32	8	291	----	* kg/cm²
5	40	32	8	442	2.89	
6	40	30	10	331	1.21	
7	40	30	10	340	1.73	
8	40	30	10	447	2.26	
9	40	30	10	571	3.05	
10	42	30	12	520	----	
11	40	26	14	325	1.31	
12	38	20	18	540	----	
13	40	20	20	372	2.64	
14	40	20	20	504	2.60	
15	40	15	25	303	----	
16	40	15	25	388	3.08	
17	40	15	25	625	3.29	
18	40	11	29	574	2.02	
19	40	10	30	501	2.47	
20	40	10	30	555	2.51	
21	40	10	30	594	1.75	
22	40	10	30	784	3.12	
23	41	10	31	669	3.10	
24	40	6	34	489	2.55	
25	40	5	35	727	2.67	
26	40	5	35	897	3.24	
27	40	0	40	427	3.02	
28	40	0	40	481	2.80	
29	40	0	40	489	----	
30	40	0	40	753	2.51	
31	40	0	40	799	3.06	

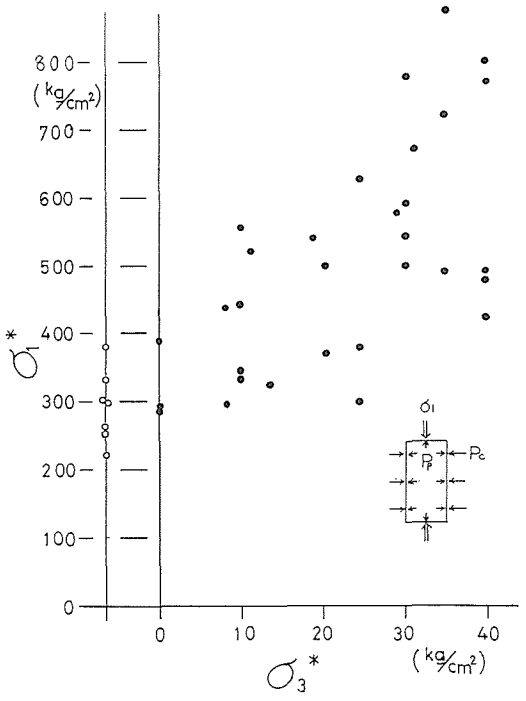

Figure 8 Relation between σ_3^* and σ_1^* of Taiheiyo coal

Table 3. Results of triaxial compression test of Sorachi coal

No.	P_c	P_p	$\sigma_3^*(P_c-P_p)$	σ_1^*	Youog's modulus ($\times 10^4$)	comment
1	40	40	0	68	0.63	Sc=139.5
2	40	32	8	131	1.69	
3	40	25	15	186	0.76	St= 5.42
4	40	15	25	199	1.64	* kg/cm²
5	40	9	31	197	1.14	
6	40	5	35	230	2.42	
7	40	0	40	269	1.20	

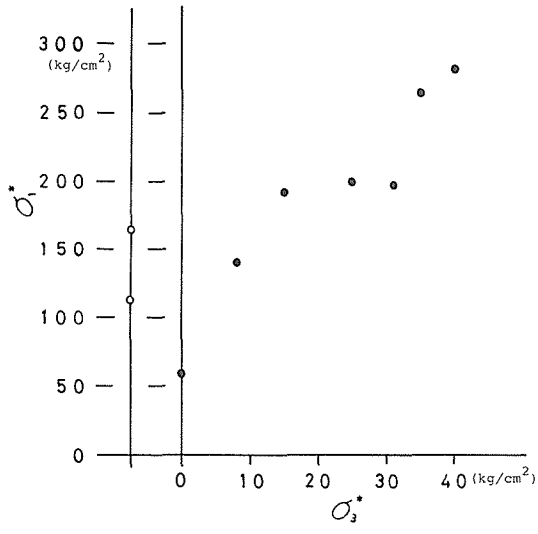

Figure 9 Relation between σ_3^* and σ_1^* of Sorachi coal

Table 4. Results of triaxial compression test of Horonai coal

No.	P_c	P_p	$\sigma_3^*(P_c-P_p)$	σ_1^*	Young's modulus ($\times 10^4$)	comment
1	40	40	0	70	0.90	Sc=140.3
2	40	40	0	139	0.78	
3	40	36	4	150	1.38	St= 13.5
4	40	35	5	111	1.34	
5	40	32	8	199	2.03	* kg/cm²
6	40	30	10	180	1.35	
7	40	25	15	175	1.53	
8	40	20	20	216	1.62	
9	40	20	20	299	2.15	
10	40	20	20	340	2.35	
11	40	20	20	343	1.80	
12	40	15	25	250	1.66	
13	40	15	25	461	3.38	
14	40	12	28	331	1.87	
15	40	12	28	342	2.36	
16	40	10	30	271	1.40	
17	40	10	30	336	1.86	
18	40	8	32	252	1.61	
19	40	8	32	320	1.65	
20	40	7	33	649	3.45	
21	40	5	35	489	2.86	
22	40	4	36	433	2.45	
23	40	0	40	496	2.50	
24	40	0	40	521	2.29	
25	40	0	40	678	3.40	

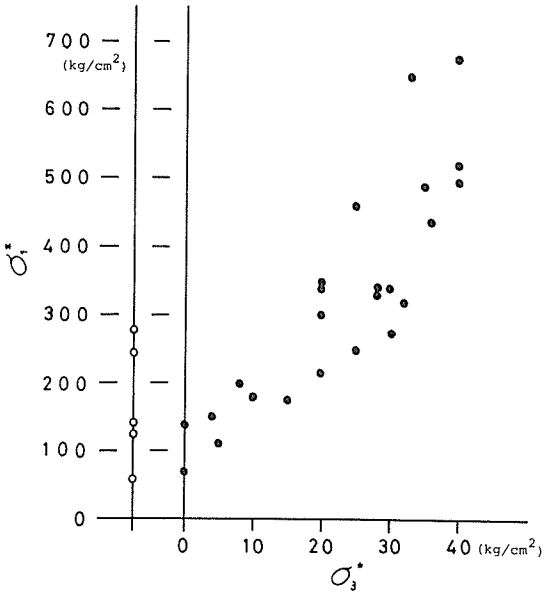

Figure 10 Relation between σ_3^* and σ_1^* of Horonai coal

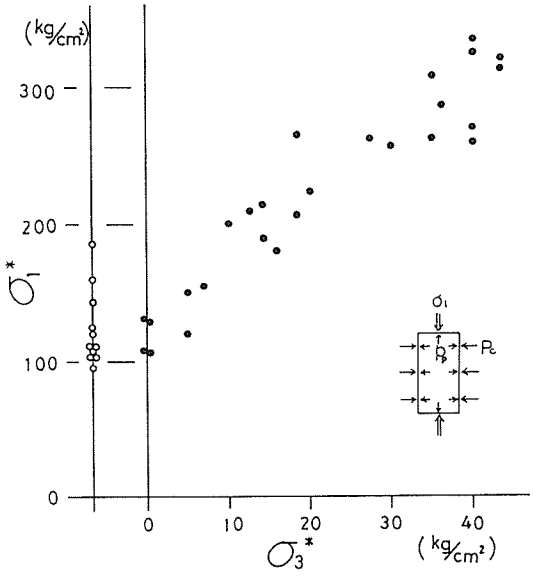

Figure 11 Relation between σ_3^* and σ_1^* of mortar

Table 5. Results of triaxial compression test of mortar

No.	P_c	P_p	$\sigma_3^*(P_c-P_p)$	σ_1^*	Young's modulus ($\times 10^4$)	comment
1	40	40	0	108	1.84	Sc=120.4
2	40	40	0	108	1.85	
3	40	40	0	129	2.32	St= 5.20
4	40	40	0	132	2.86	
5	40	35	5	120	1.48	* kg/cm²
6	40	35	5	151	2.50	
7	41	34	7	166	1.63	
8	40	30	10	207	2.48	
9	40	27	13	210	2.75	
10	40	26	14	189	2.68	
11	44	30	14	216	2.93	
12	40	24	16	181	2.45	
13	40	22	18	208	3.01	
14	40	22	18	271	3.47	
15	40	20	20	223	2.47	
16	40	13	27	263	----	
17	40	10	30	258	2.47	
18	40	5	35	262	----	
19	40	5	35	309	2.14	
20	40	4	36	288	----	
21	40	0	40	258	----	
22	40	0	40	271	2.87	
23	40	0	40	324	3.08	
24	40	0	40	326	----	
25	45	0	45	313	2.96	
26	45	0	45	319	3.26	

Table 5 shows the experimental results of mortar. The average uniaxial compressive strength of mortar was 120.4 Kg/cm^2, its average tensile strength was 5.2 Kg/cm^2 and porosity was 22.4 %. Figure 11 shows the relation between σ_3^* and σ_1^*. When the pore gas pressure was increased, the strength of the mortar decreased distinctly. The ratio of the strength at $\sigma_3^*=0$ against that at $\sigma_3^*=40$ Kg/cm^2 was about 1/3 compared with the most far apart values in Table 5. When $\sigma_3^*=0$, triaxial compressive strength was nearly equal to the uniaxial compressive strength.

It was experimentally confirmed that if the pore gas pressure was applied to the coals in the triaxial compression test under the constant confining pressure condition, failure stress σ_1^* decreased definitely and σ_1^* when $\sigma_3^*=0$ became almost equal to the uniaxial compressive strength.

5. Consideration of experimental results

Up to here, it was described provisionally that $\sigma_3^*=P_c-P_p$. More correctly, σ_3^* should be written as

$$\sigma_3^*=P_c-\alpha P_p \qquad (0\leqq\alpha\leqq 1) \tag{1}$$

where, α is the coefficient of pore pressure effectiveness (refer to Figure 12).

The value of α could be decided in the following manner.

With reference to Figure 13, failure criterion is decided as

$$\tau^2=mT_0(T_0-\sigma) \tag{2}$$

where, m : Constant given both from uniaxial compressive strength and tensile strength.

T_0 : Tensile strength.

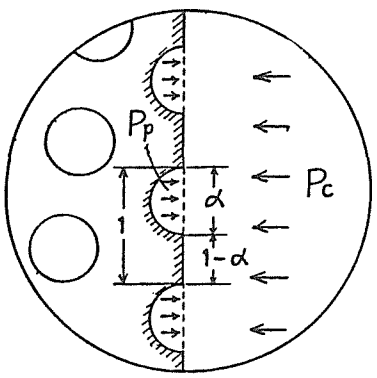

Figure 12 Effectiveness of pore pressure

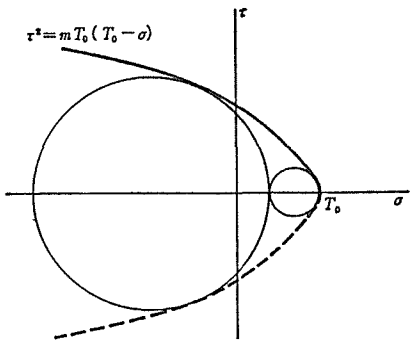

Figure 13 Parabolic envelope for failure criterion

Stress state of material could be given

$$\tau^2+\left(\sigma-\frac{\sigma_1+\sigma_3}{2}\right)^2=\left(\frac{\sigma_1-\sigma_3}{2}\right)^2 \tag{3}$$

Eq. (3) could be rewritten

$$\tau^2+(\sigma-h)^2=\tau_m{}^2 \tag{4}$$

provided that

$$\frac{\sigma_1-\sigma_3}{2}=\tau_m,\quad \frac{\sigma_1+\sigma_3}{2}=h$$

To derive the failure conditions under triaxial stresses, from Eqs. (2) and (4) we get

$$(\sigma-h)^2+m\ T_0(T_0-\sigma)=\tau_{m^2} \tag{5}$$

From Eq. (5), equal root condition for σ can be given

$$\tau_{m^2}+T_0h+m\left(\frac{m}{4}-1\right)T_0^2=0 \tag{6}$$

Eq. (6) can be rewritten

$$\left(\frac{\sigma_1-\sigma_3}{2}\right)^2+mT_0\left(\frac{\sigma_1+\sigma_3}{2}\right)+m\left(\frac{m}{4}-1\right)T_0^2=0 \tag{7}$$

Solving Eq. (7) for σ_1, it follows that

$$\sigma_1=\frac{1}{2}\left[(\sigma_3-mT_0)\pm\{(mT_0)^2-4mT_0\sigma_3-m(m-4)T_0^2\}^{1/2}\right] \tag{8}$$

Eq. (8) shows that if the equation of Mohr envelope for failure criterion is decided and the confining pressure σ_3 is given, the axial stress σ_1 for failure without pore gas pressure can be evaluated.

In the case where pore gas pressure is applied, the failure condition follows that

$$\sigma_1^*=\frac{1}{2}\left[\{(P_c-\alpha P_p)-mT_0\}\pm\{(mT_0)^2-4(mT_0)(P_c-\alpha P_p)-m(m-4)T_0^2\}^{1/2}\right] \tag{9}$$

When $\sigma_3=0$ in Eq. (8), it means that uniaxial compression test is conducted. Then Eq. (8) can be written

$$\sigma_1=\frac{1}{2}\left[-mT_0\pm\{(mT_0)^2-m(m-4)T_0^2\}^{1/2}\right] \tag{10}$$

While, assuming that $\alpha=1$, $P_c=P_p$ in Eq. (9) in triaxial compression test, Eq. (9) can be written

$$\sigma_1^*=\frac{1}{2}\left[-mT_0\pm\{(mT_0)^2-m(m-4)T_0^2\}\right] \tag{11}$$

The right sides of Eqs. (10) and (11) are equal to each other.

Experimentally, it has been confirmed that if $P_c=P_p$, uniaxial compressive strength S_C was almost equal to failure stress σ_1^* in triaxial compression test. Namely, we can say that Law of Effective Stress could be almost absolutely applied to employed coals like in the case of soil mechanics.[5]

6. Conclusion

(1) In the triaxial compression test using three sorts of coals and one kind of mortar, if the pore gas pressure was applied under the constant confining pressure, the failure stress σ_1^* dropped clearly. It can be said that these results are as same as the results conventionally conducted under water pressure applied test.

(2) From equal root condition between equations of Mohr's circle and Mohr envelope, it was evaluated $\alpha\fallingdotseq 1$ and confirmed that Law of Effective Stress can be fitted to coals almost absolutely.

(3) Under the constant confining pressure i. e. $P_c=40$ Kg/cm^2, it was found that according to the pore gas pressure change, fracture form changes reversibly as follow :

Pore gas pressure increase
(Ductile fractare) $\rightleftharpoons$ (Brittle fracture)
Pore gas pressure decrease

Among the above mentioned terms, (1) involves the most important factors. It shows that if the other environmental conditions nearby working are immutable, the more the pore gas pressure increases, the more the movement of Mohr's circle toward origin becomes remarkable and the part of the coal seam readily reverts to shearing and pulverization. If these pulverizations occurred instantaneously at the back of the face, one of the conditions for coal and gas outbursts might be caused.

7. Acknowledgement

The authors would like to express their thanks for the academic advice by emeritus Prof. T. Isobe and for the assistance in this study by T. Shiohata and Y. Kamiyama, graduate students of Hokkaido University.

Literatures Cited

1) Y. Hiramatsu, *J. Min. Metal. Inst. Jap.*, 98 (1136)pp 989-991 (1982)
2) J. Handin et al, *Bull. Ame. Assoc. Petro. Geol.*, 47 pp 717-755 (1963)
3) W. F. Brace et al, *Int. J. Rock Mech. Min. Sci.* 5 (5) pp 415-426 (1968)
4) T. Goto et al, *J. Min. Metal. Inst. Jap.*, 98 (1131) pp 393-398 (1982)
5) J. C. Jager and N. G. W. Cook, *Fundamental of Rock Mechanics,* Chapman and Hall, pp 214-225 (1968)